Materials Research Letters

ISSN: (Print) (Online) Journal homepage: www.tandfonline.com/journals/tmrl20

Mapping stress heterogeneity in single-crystal superalloys by novel submicron-resolved X-ray diffraction

Jiawei Kou, Kai Chen, Shaoqi Huang, Chongpu Zhai, Ching-Yu Chiang, Sisheng Wang, Zhijun Li & Yan-Dong Wang

To cite this article: Jiawei Kou, Kai Chen, Shaoqi Huang, Chongpu Zhai, Ching-Yu Chiang, Sisheng Wang, Zhijun Li & Yan-Dong Wang (2024) Mapping stress heterogeneity in single-crystal superalloys by novel submicron-resolved X-ray diffraction, Materials Research Letters, 12:6, 450-458, DOI: 10.1080/21663831.2024.2341932

To link to this article: https://doi.org/10.1080/21663831.2024.2341932

MATER. RES. LETT.
2024, VOL. 12, NO. 6, 450–458
https://doi.org/10.1080/21663831.2024.2341932

MATERIALS RESEARCH LETTERS
Taylor & Francis
Taylor & Francis Group

ORIGINAL REPORT

Mapping stress heterogeneity in single-crystal superalloys by novel submicron-resolved X-ray diffraction

Jiawei Kou[a], Kai Chen [a], Shaoqi Huang[b], Chongpu Zhai[b], Ching-Yu Chiang[c], Sisheng Wang[d], Zhijun Li[e] and Yan-Dong Wang[f,g]

[a]Center for Advancing Materials Performance from the Nanoscale (CAMP-Nano), State Key Laboratory for Mechanical Behavior of Materials, Xi'an Jiaotong University, Xi'an, People's Republic of China; [b]State Key Laboratory for Strength and Vibration of Mechanical Structures, School of Aerospace Engineering, Xi'an Jiaotong University, Xi'an, People's Republic of China; [c]Scientific Research Division, National Synchrotron Radiation Research Center, Hsinchu, Taiwan, Republic of China; [d]Shanghai Synchrotron Radiation Facility, Shanghai Advanced Research Institute, Chinese Academy of Sciences, Shanghai, People's Republic of China; [e]Shanghai Institute of Applied Physics, Chinese Academy of Sciences, Shanghai, People's Republic of China; [f]Beijing Advanced Innovation Center for Materials Genome Engineering, State Key Laboratory for Advanced Metals and Materials, University of Science and Technology Beijing, Beijing, People's Republic of China; [g]Institute of Materials Intelligent Technology, Liaoning Academy of Materials, Shenyang, People's Republic of China

ABSTRACT

Coherent precipitation, a common strengthening approach, is typically subjected to spatial non-uniformity due to microscopic segregation, leading to multi-scale stress heterogeneity. Such heterogeneity remains poorly characterized because unavailable local strain-free lattice parameters invalidate traditional diffraction-based stress measurement techniques. To overcome these limitations, we demonstrate a submicron-resolved synchrotron X-ray diffraction method to map coherency stress distribution based on the γ/γ' lattice misfits in Ni-based superalloys. Assisted by finite element analysis, sub-dendritic stresses are deduced from heterogeneous coherency stresses, confirmed by the diffraction experiments. The methodology offers a comprehensive framework to assess stress heterogeneity at multi-scales for all coherent precipitation strengthened alloys.

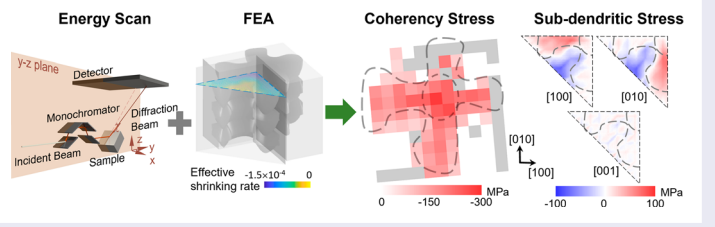

IMPACT STATEMENT

This study marks the first successful quantification of stress heterogeneity at multi-scales in alloys strengthened by non-uniform coherent precipitation, even in absence of strain-free lattice constants.

ARTICLE HISTORY
Received 19 February 2024

KEYWORDS
Stress heterogeneity mapping; submicron-resolved X-ray diffraction; nonuniform coherent precipitation; Ni-based single crystal superalloys; finite element analysis

1. Introduction

Coherent precipitation has long been employed to strengthen materials across a wide temperature range [1,2]. In recent years, spatially hierarchical and/or nonuniform coherent precipitation has been proposed to achieve unprecedented mechanical properties [3–6]. The stress heterogeneity at multiple scales, induced by inhomogeneously distributed chemical compositions and coherency stresses, plays a key role in determining the mechanical performance [7–10]. Thus, mapping the heterogeneous stresses favors the understanding and design of such alloys. Among various stress characterization techniques, X-ray diffraction is the most widely applied for its accuracy and feasibility [11,12]. Yet, in dealing with heterogeneous materials, traditional diffraction techniques are facing formidable challengesbecause

CONTACT Kai Chen kchenlbl@gmail.com Center for Advancing Materials Performance from the Nanoscale (CAMP-Nano), State Key Laboratory for Mechanical Behavior of Materials, Xi'an Jiaotong University, Xi'an, Shaanxi 710049, People's Republic of China; Yan-Dong Wang ydwang@ustb.edu.cn Beijing Advanced Innovation Center for Materials Genome Engineering, State Key Laboratory for Advanced Metals and Materials, University of Science and Technology Beijing, Beijing 100083, People's Republic of China Institute of Materials Intelligent Technology, Liaoning Academy of Materials, Shenyang, Liaoning 110004, People's Republic of China

Supplemental data for this article can be accessed online at https://doi.org/10.1080/21663831.2024.2341932.

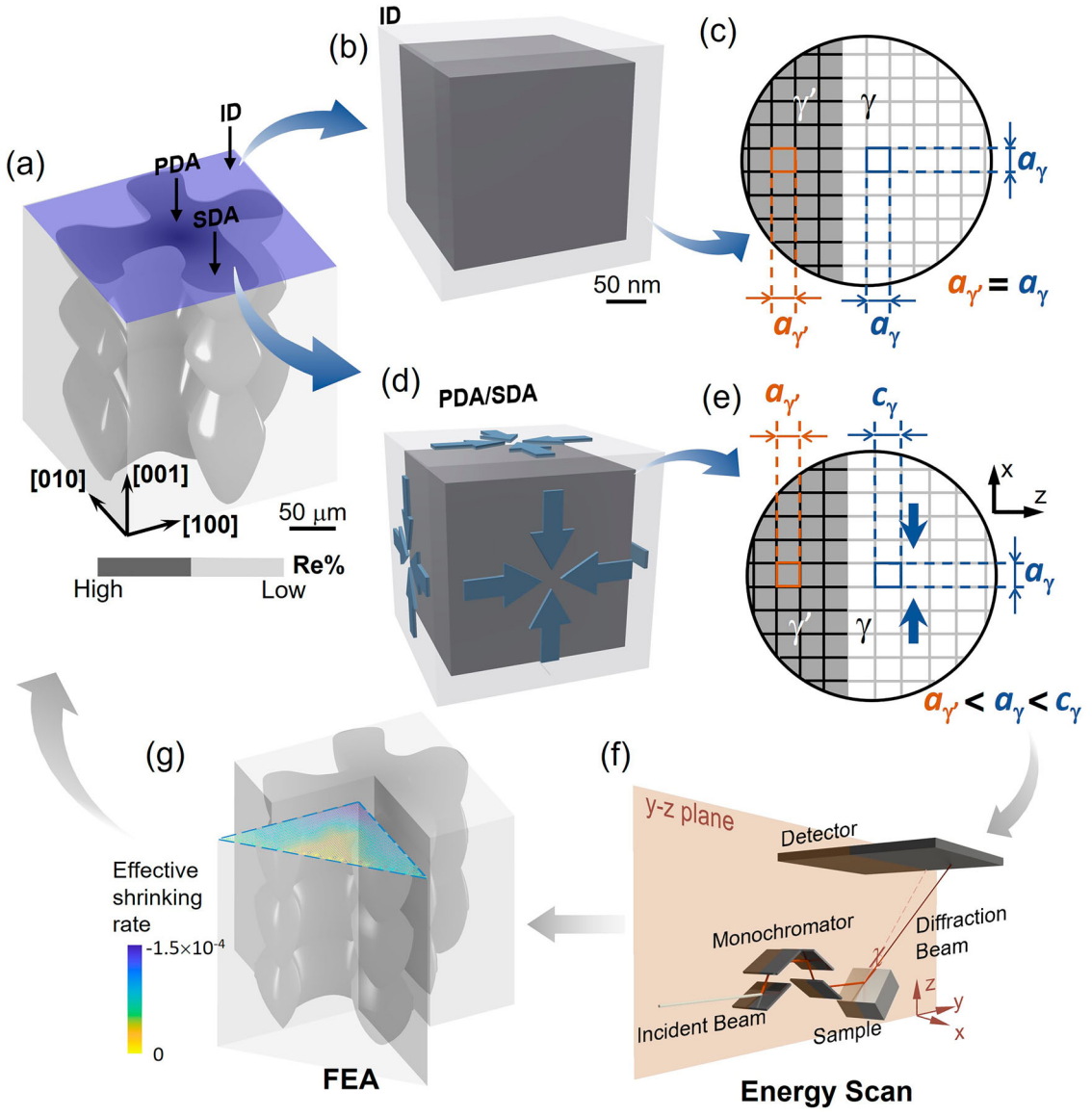

Figure 1. The methodology on stress heterogeneity investigation. (a) The dendritic structure of the NBSC superalloys is demonstrated schematically, and the shadow indicates the characterized cross-section. (b-e) Lattice misfit and coherency stress are significantly non-uniform from the ID regions to the PDAs/SDAs. In ID, almost undetectable coherency stress is induced (b) because the lattices of γ' and γ phases are almost the same (c). In PDAs/SDAs, biaxial compressive coherency stress is induced in the γ-channels (d) because the lattice of γ-phase is slightly larger than that of γ'-phase, and tetragonal distortion is generated in the γ-channels (e). (f) Submicron-resolved diffraction technique is applied for lattice misfit and coherency stress mapping. (g) The so-called effective shrinkage rate is obtained from diffraction data and employed for finite element modeling to study the sub-dendritic stress distribution.

the element segregation and stress partitioning result in locally varied and unknown standard 'strain-free' lattice parameters [13,14].

Ni-based single crystal (NBSC) superalloys, a typical alloy featured by cuboidal shaped γ'-precipitates coherently embedded in γ-matrix that is strengthened by dozens of solid-solution elements. The high contents of various refractory elements persist in sub-dendritic scale segregation even after industrial standard heat treatment [15–17]. The micro-segregation leads to nonuniform coherency stresses and consequent inhomogeneous sub-dendritic stresses among primary/secondary dendrite arms (PDAs/SDAs) and interdendritic (IDs) regions (Figure 1a–e), which result in significant deformation heterogeneity, i.e. asynchronous and location-dependent rafting [18–20], fatigue behaviors [21] and recovery ability [22–25]. Because the sub-dendritic micro-segregation, lattice misfit and stress heterogeneity are a complicated function of chemical composition, fabrication techniques, as well as thermomechanical history [26], barely any successful characterization of local stress in superalloys has been reported.

While synchrotron-based Laue diffraction has been employed to probe stress in various materials [27–32], including NBSC superalloys [22–25,30], its limited capability in distinguishing γ and γ' phases, as well as in measuring dilatational strains, has restricted its applications in analyzing lattice misfit and stress heterogeneities at scales ranging from individual precipitates to entire dendrites.

In this study, we propose a novel submicron-resolved synchrotron X-ray diffraction-based approach to map the multi-scale stress heterogeneity, circumventing the determination of unconstrained lattice constants. This marks the first achievement of local coherency stress measurement in NBSC superalloys. Moreover, stresses at the sub-dendritic scale, which is typically infeasible to measure directly, are deduced from the coherency stress maps combined with finite element analysis (FEA) and validated with the micro-Laue results. The approach developed here has a broad implication for coherent precipitation hardened alloys, including refractory and high-entropy ones that are being intensely pursued for applications under harsh service conditions.

2. Materials and methods

The stress heterogeneity is investigated on a typical 2nd generation CMSX-4 NBSC superalloy, in which the primary dendrite arms (PDAs) grow approximately along [001] direction, while the secondary dendrite arms (SDAs) along [100] and [010]. The specimen discs are sliced parallel with the (001) plane from a cast boule, and then subjected to a standard heat treatment, including a two-step super-solvus solutionizing annealing at 1290°C for 3 h and then 1300°C for 6 h, followed by aging annealing at 1140°C for 2 h and 870°C for 20 h, and finally air cooled to ambient temperature [13]. After heat treatment, a 5 mm × 5 mm × 3 mm (length × width × thickness) bulky specimen is cut from the disc and the surface is electrical polished. Even after heat treatment, a cross-shaped dendrite structure, approximately 300 μm in size, remains discernible (schematically shown in Figure 1a) probably due to the micro-segregation of refractory elements like Re (will be displayed in Figure 3a, mapped by wavelength-dispersive X-ray spectroscopy). The spatial distribution of the side length of the cuboidal γ'-precipitates and the width of the slender γ-channels is investigated in detail (Supplementary Information Section A).

Because of the element segregation, the lattice misfit, and thus the coherency stress, is spatially inhomogeneous (Figure 1b–e). To investigate the stress heterogeneity, a novel submicron-resolved diffraction is carried out using the synchrotron radiation-based X-ray beam that is focused into ~100 nm in diameter (Figure 1f). The specimen is mounted on a high-resolution scanning stage, 45° tilted relative to the incident beam, and carefully positioned at the X-ray focal point. A 330 µm × 330 µm surface area, encompassing a cross-shaped dendrite as indicated by the blue shadowed region in Figure 1a, is scanned using the polychromatic (5–30 keV) X-ray probe with 15-µm step size and 0.05 s exposure. At each scanning position, a Laue pattern is recorded by a 2D DECTRIS Pilatus-6M detector that is placed 520 mm above the specimen. The Laue patterns are indexed and the energy of the 004 reflection, although varying from pattern to pattern, is determined to be roughly 10,180 eV. Subsequently, the energy-adjustable monochromator is inserted into the X-ray pathway to execute 004-reflection energy scan. The identical area is scanned again, but with a step size of 30 µm, since energy scans are more time-consuming than Laue scans. At each position, the incident X-ray beam energy is scanned from 10,023 to 10,293 eV with a 2-eV step, and the diffraction signal is recorded with 0.1 s exposure at each energy. In the meantime, a scanning electron microscope (SEM) image of the energy scanned position is captured to measure the local volume fraction of γ'-phase. The Laue diffraction and energy scan data are analyzed using a custom-developed software *PYXIS* [33]. For Laue scans, *PYXIS* can search and index peaks on each individual Laue pattern automatically to obtain the local orientation and deviatoric strain tensor. For energy scan data, *PYXIS* can reconstruct the peak in 3D, and then fit and determine the subpeak position for accurate lattice constant measurement.

Afterwards, 1/8 of the scanned area is subtracted for FEA. The so-called effective shrinking rate is defined based on the experimentally mapped lattice misfit distribution, from which the sub-dendritic stress distribution is obtained (Figure 1g). Detailed results from the submicron-resolved diffraction and FEA are demonstrated in the next section.

3. Results and discussion

The stresses imposed onto γ and γ' phases are generated from their lattice misfit. Based on the submicron-resolved diffraction results, the coherency stresses in the ID zones are quite different from those in the PDA/SDA regions. In Figure 2a1, some of the diffraction profiles of the 004-reflection recorded in the ID region at various energies are displayed. For better visualization, a coordinate system, θ-χ-$\boldsymbol{q}$, is established, in which θ is the Bragg angle, χ the azimuthal angle and $|\boldsymbol{q}|$ the length of the scattering vector (more details in Supplementary

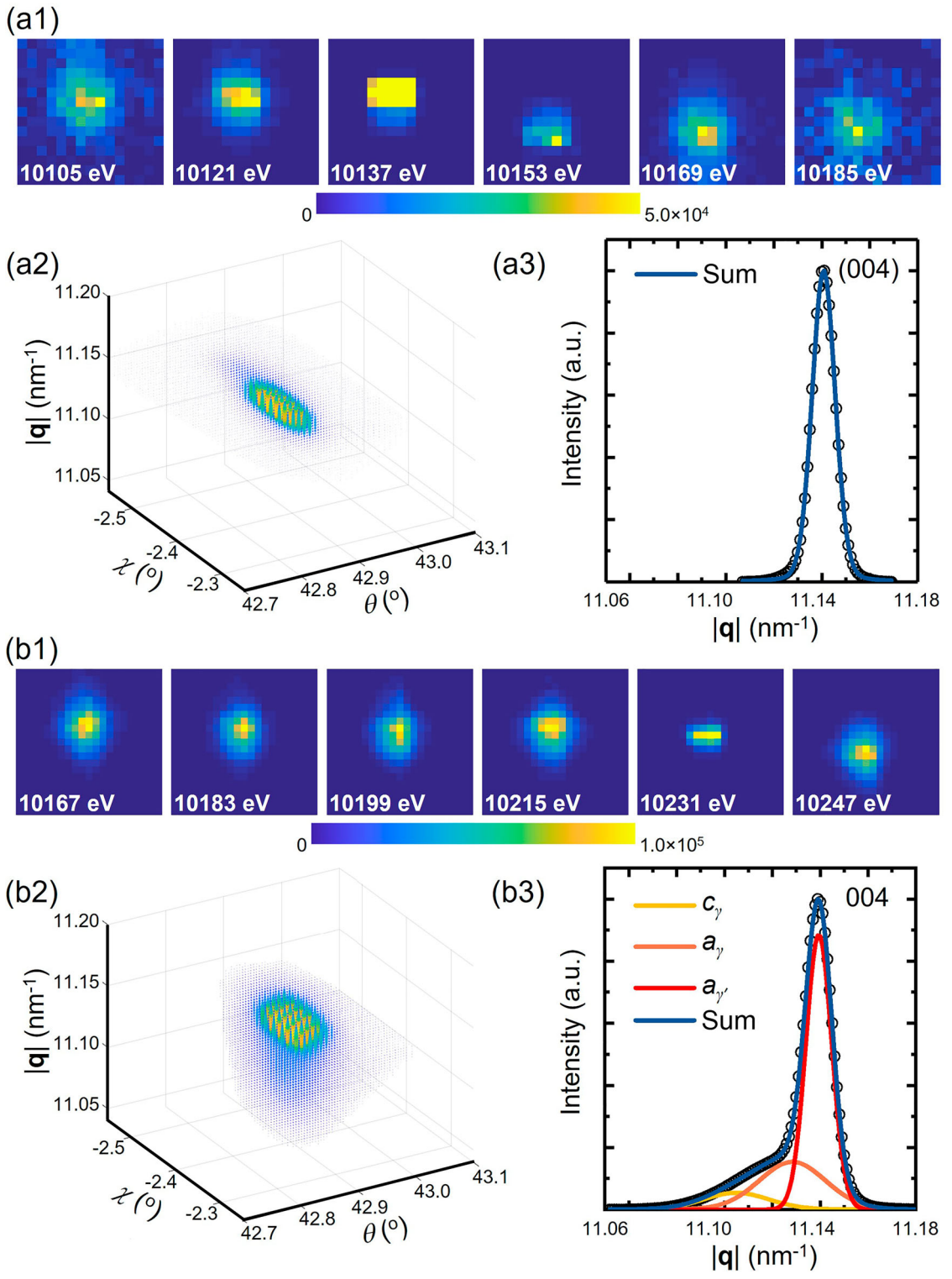

Figure 2. γ/γ' lattice misfit measurements for (a) ID and (b) PDA/SDA regions. For each spot, a series of diffraction signals are recorded from energy scan experiments (Panel 1), which are then reconstructed in 3D (Panel 2) and finally projected to obtain a 1D peak profile (Panel 3).

Section B). Each pixel on the series of diffraction patterns recorded in the energy scan is converted to the θ-χ-$\boldsymbol{q}$ coordinates, resulting in the 3D reconstructed 004-reflection (Figure 2a2). The intensity variation of the peak is color-coded, with blue indicating the lowest and red the highest. Subsequently, the peak profile is projected onto the $|\boldsymbol{q}|$ axis, shown by the black circles in Figure 2a3. In most of the scanned positions in the ID

region, the diffraction peak is symmetric as this one, indicating that the lattice misfit is below the resolving capability of the synchrotron diffraction technique. In these cases, the γ and γ' phases are believed to possess the same lattice parameters. Then a pseudo-Voigt function is applied to determine the peak position (blue curve) and calculate the lattice constant. In several positions in the ID area, multiple diffraction peaks are recorded because the X-ray beam penetrates more than one dendrite which is slightly misoriented. For them a Gaussian Mixture Model-Expectation Maximization (GMM-EM) method [34] is employed to separate the partially overlapped peaks (Supplementary Section C).

In the PDA and SDA areas, the peak profiles are significantly different. A typical energy scan recorded in PDA is demonstrated in Figure 2b1, and the data is treated in a similar way to those taken in ID. In 3D, a weak peak is noticed hiding under a strong one in the low $|\boldsymbol{q}|$ direction (Figure 2b2), which can also be visualized in the 1D projection (Figure 2b3). The lower $|\boldsymbol{q}|$ peak is from the γ phase, indicating that the γ-matrix has larger unit cells than the γ'-particles. To fit the peak profile reasonably and accurately, the stress/strain status of both γ and γ' phases are analyzed.

As demonstrated in Figure S1, the widths of the γ-channels in the heat-treated NBSC superalloys are always smaller than 1/7 of the side lengths of the cuboidal γ'-particles, thus it is reasonable to simplify the γ-channels as thin flat plates under equi-biaxial compressive stresses, and hydrostatic tensile stresses are imposed onto the γ'-precipitates. Such stress conditions lead to a tetragonal distortion in the γ-phase lattices, i.e. the lattice constant perpendicular to the interphase boundary (c_γ) is wider than the other two lattice constants (a_γ). The γ'-particles remain their cubic symmetry, and thus only one lattice constant $a_{\gamma'}$ needs to be determined. Therefore, the peak profile in Figure 2b3 is fitted using three pseudo-Voigt functions. Moreover, the volume fraction of γ' phase can be computed by the equation $f_{\gamma'} = \left(\frac{r \cdot A_{\gamma,2} + A_{\gamma'}}{r \cdot A_{\gamma,1} + r \cdot A_{\gamma,2} + A_{\gamma'}}\right)^3$, where $A_{\gamma'}, A_{\gamma,1}$ and $A_{\gamma,2}$ are the area of the fitted peak for lattice constants $a_{\gamma'}$, c_γ and a_γ, respectively, and the factor r is the square of the structure factor ratio between γ' and γ phases (details in Supplementary Section D). To ensure accurate peak fitting, the volume fraction of γ' phase derived from peak areas is validated with the SEM images recorded when the diffraction patterns were collected.

Once the lattice constants are obtained from peak fitting, the coherency stress and lattice misfit are ready to be calculated. For γ-channels under tetragonal distortion, various lattice misfits are defined [35–39]. Here we adopt the simplest definition of constrained lattice misfit δ [39]:

$$\delta = \frac{2(a_{\gamma'} - a_{\gamma,cub})}{a_{\gamma'} + a_{\gamma,cub}}, \tag{1}$$

where $a_{\gamma,cub}$ is the lattice constant of unstrained and unconstrained γ-phase. Derived in Supplementary Section E, $a_{\gamma,cub}$ can be calculated by:

$$a_{\gamma,cub} = \frac{(1-\upsilon)\cdot c_\gamma + 2\upsilon \cdot a_\gamma}{1+\upsilon}, \tag{2}$$

where υ is the Poisson ratio of γ-phase, taken as 0.38 [36]. The coherency stress imposed onto the γ-channels σ_{coh} can be computed following:

$$\sigma_{coh} = E_{[001]} \cdot \frac{a_\gamma - c_\gamma}{(1-\upsilon)\cdot c_\gamma + 2\upsilon \cdot a_\gamma}, \tag{3}$$

where $E[001]$ is the Young's modulus of γ-phase in the [001] direction (139 GPa) [40].

The sub-dendrite scale distributions of lattice misfit and coherency stress are studied. The PDA and SDA are delineated based on the micro-segregation of Re, as shown in Figure 3a. The constrained lattice misfit and the coherency stress in the γ-channels are plotted in Figure 3b and c, respectively. Gray pixels denote position without valid diffraction data due to surface voids, and white pixels represent symmetrical diffraction peak profiles, in which γ- and γ'-phases cannot be resolved. The transition from PDA/SDA to ID is abrupt. The lattice misfit in SDA ranges from -0.5×10^{-3} to -1.5×10^{-3}. In PDA, the lattice misfit is consistently below -1.5×10^{-3}, with the lowest at -2.6×10^{-3}. Induced by the lattice misfit, the coherency stress in γ-channels within SDA is approximately 150 MPa, and above 200 MPa in PDA.

As mentioned, the sub-dendritic stress cannot be mapped by the conventional method since no stress-free lattice constants can be referred to. A novel strategy is proposed here to map the sub-dendritic stress based on the local lattice misfit, without knowing the lattice constants. It is assumed that the stresses at the sub-dendritic scale are completely resulted from the stark heterogeneities on coherency stress from the PDA/SDA to the ID regions. A comprehensive finite element model is constructed using the elements of cuboidal units, each of which comprises a γ'-particle embedded by γ-channels with half of their width. To count the coherency stress inhomogeneity, each element shrinks by a rate of $\frac{a_\gamma - a_{\gamma,cub}}{a_{\gamma,cub}}$, which is measured and computed from the diffraction data, and called 'effective shrinking rate' in this study. This is a surrogate for the cooling process of

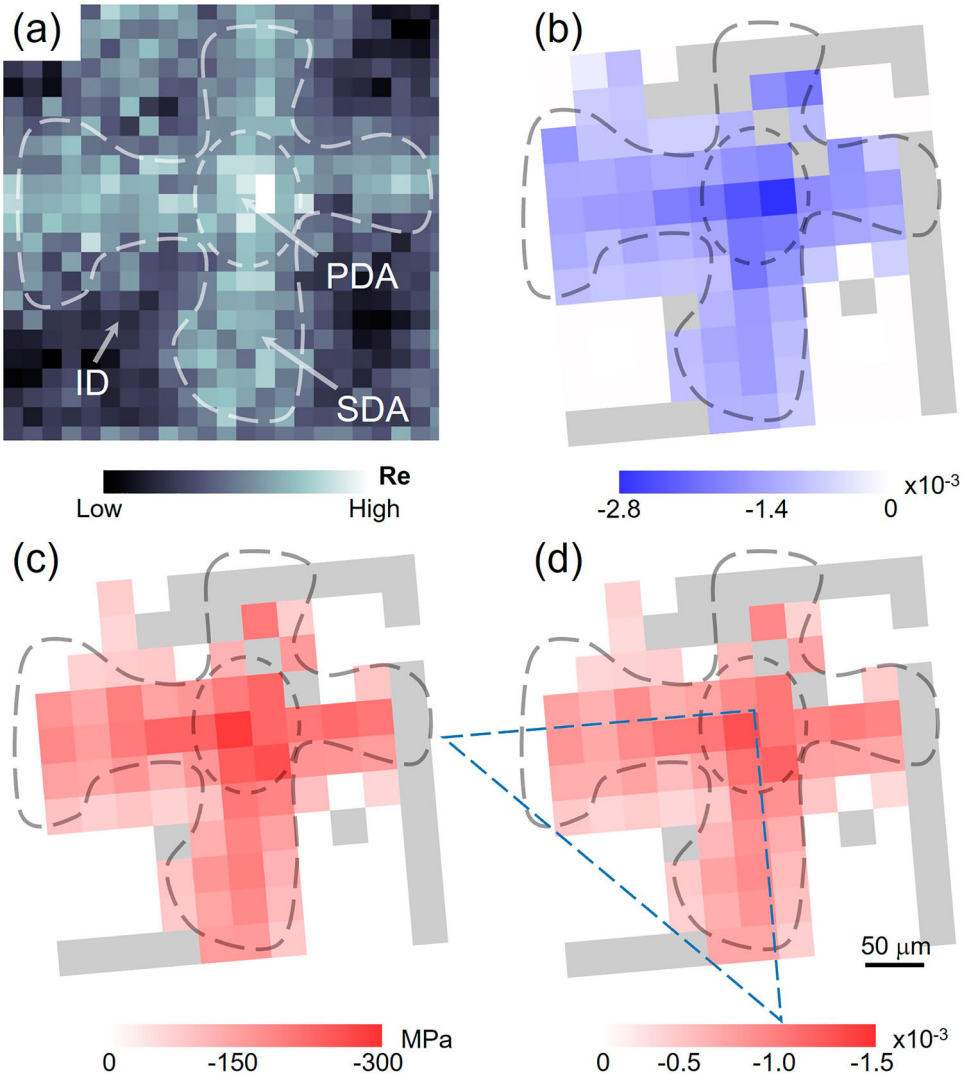

Figure 3. Heterogeneously distributed lattice misfit and coherency stress in the heat-treated NBSC superalloy. (a) The micro-segregation of Re element delineates the regions of PDA, SDAs and ID structure. The distributions of constrained lattice misfit (b), equi-biaxial coherency stress in γ -channels (c) and effective shrinking rate (d) are dependent on the dendritic structure.

an object with the locally varied coefficient of thermal expansion, and the concept and methodology have been well-established with FEA. Owing to the symmetry of the cross-shaped pattern, only the triangular section delineated by blue dashed lines in Figure 3d is modeled. Since the mesh in the FEA is smaller than the diffraction scanning step size, the effective shrinking rate at some mesh points is interpolated naturally. For boundary conditions, the two right-angle sides, which are parallel to the [100] and [010] directions, and the face, parallel to the (001) crystallographic plane, are designated as free, while the hypotenuse is treated as a symmetric boundary (more details in Supplementary Section F).

Maps in Figure 4a depict the stresses at the sub-dendritic scale along [100], [010] and [001] directions, respectively. Dashed lines in these figures indicate the boundaries of PDA and SDA. On the (001) plane, the ID region is subjected to $\sim$60 MPa biaxial compressive stress, while the PDA zone experiences tensile biaxial stress of about 30 MPa. In the SDA area, tensile stresses of approximately 60 MPa are imposed along the dendrite arm directions. In contrast, almost no stress prevails along [001] direction for both dendrite and interdendrite areas.

To validate the modeling and simulation, deviatoric strains are deduced from FEA and compared with those measured from the submicron-resolved Laue diffraction data. From the deviatoric strain components along $<001>$ directions, the FEA results (Figure 4b) are consistent with the experimental ones (Figure 4c).

It is worth noticing that the sub-dendritic stresses obtained in this study are significantly different from the

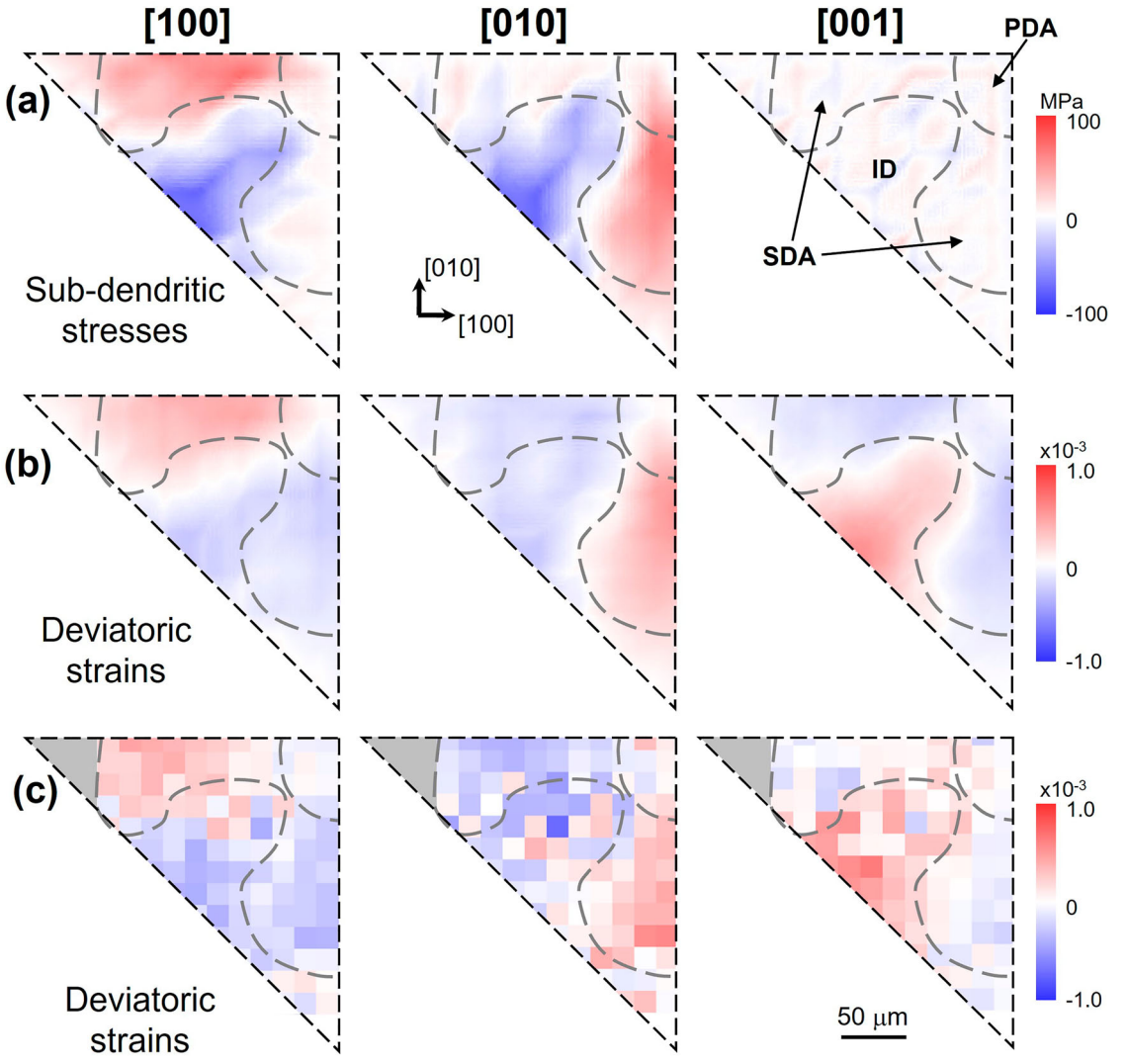

Figure 4. The sub-dendritic stress and deviatoric strain distributions along [100], [010] and [001] directions, with dashed gray curves indicating the PDA, SDA and ID regions. (a) The sub-dendritic stresses are obtained from the finite element modeling, the validity of which is cross-checked by comparing the deviatoric strains computed from the FEA outputs (b) and those from submicron-resolved diffraction experiments (c).

previously reported ones, in terms of both magnitude and sign [20]. In that work, although the sub-dendritic stresses were also simulated from FEA, the coherency stresses in γ -channels was not considered in modeling, and the X-ray diffraction experiment employed there for validation did not exhibit enough spatial resolution. Thus, the results in the present study are more reliable.

The consistency between FEA modeling and experimental measurement supports the conclusion that in the exampled heat-treated NBSC superalloys, the stresses at the sub-dendritic scale originate from the heterogeneity on the coherency stress, which is induced by the non-uniformly distributed lattice misfit from PDA/SDA to ID. For NBSC superalloys, as well as a wide range of engineering materials, the absence of unconstrained lattice constants hampers stress mapping, and thus the property and service life prediction. This study proposes a novel approach to deduce the Type II microscale stresses by mapping the heterogeneous distributions of the nanoscale Type III coherency stresses, as demonstrated by Figure 1. For alloys with relatively low precipitate volume fraction, the thin flat plate approximation might not be fulfilled, and thus the stresses are no longer equi-biaxial; however, the strategy developed here is still valid, except that the energy scan experiments must be carried out on more diffraction peaks to calculate the stress tensor. For deformed alloys, the local stress status will be greatly dependent of dislocation density, distribution and configuration. Thus, the assumptions and modeling employed in this study may need modification based on the characterizations of dislocations using other techniques such as transmission electron microscopy.

4. Conclusions

In the present study, the lattice misfit and the coherency stress in a fully heat-treated NBSC superalloy, CMSX-4, have been mapped using a novel submicron-resolved diffraction technique, which has not been achieved before by any experimental approaches. The stress distribution at the sub-dendritic scale, caused by the coherency stress heterogeneity, is deduced with the assistance of FEA modeling and measured local effective shrinking rate. Our results show the coherency stress peaks at over 200 MPa in PDA, and reaches around 150 MPa in SDA. In contrast, most ID regions show an absence of lattice misfit and coherency stress. Such heterogeneity leads to uniaxial stress of up to 60 MPa along the SDA and similar levels of biaxial stress onto ID within the (001) plane. However, for both dendritic and interdendritic regions, no stress prevails along [001] direction in which the PDA grows. The present approach enables precise mapping of heterogeneity in coherency stress, along with the resultant microscale stress, at a spatial resolution limited by the synchrotron X-ray beam size.

Acknowledgements

We thank Instrumental Analysis Center of Xi'an Jiaotong University and Dr. Chuanwei Fan from CAMPNano for technical support.

Disclosure statement

No potential conflict of interest was reported by the author(s).

Funding

This work is supported by the National Science and Technology Major Project (2019-VII-0019-0161), the National Key Research and Development Program of China (No. 2021YFA1600600), the National Natural Science Foundation of China (grant number U2032205, 51927801 and 52271042), and the Outstanding Young Scholar Program (2020-JCJQ-009).

ORCID

Kai Chen http://orcid.org/0000-0002-4917-4445

References

[1] Nemoto M, Tian W, Sano T. Coherent precipitation strengthening by/in LI2-ordered phases. J Phys III. 1991;1(6):1099–1117. doi:10.1051/jp3:1991174

[2] Pollock TM, Tin S. Nickel-based superalloys for advanced turbine engines: chemistry, microstructure and properties. J Propul Power. 2006;22(2):361–374. doi:10.2514/1.18239

[3] Kürnsteiner P, Wilms MB, Weisheit A, et al. High-strength Damascus steel by additive manufacturing. Nature. 2020;582(7813):515–519. doi:10.1038/s41586-020-2409-3

[4] Du X, Li W, Chang H, et al. Dual heterogeneous structures lead to ultrahigh strength and uniform ductility in a Co-Cr-Ni medium-entropy alloy. Nat Commun. 2020;11(1):2390. doi:10.1038/s41467-020-16085-z

[5] Jang TJ, Choi WS, Kim DW, et al. Shear band-driven precipitate dispersion for ultrastrong ductile medium-entropy alloys. Nat Commun. 2021;12(1):4703. doi:10.1038/s41467-021-25031-6

[6] Zhao Y, Yang T, Tong Y, et al. Heterogeneous precipitation behavior and stacking-fault-mediated deformation in a CoCrNi-based medium-entropy alloy. Acta Mater. 2017;138:72–82. doi:10.1016/j.actamat.2017.07.029

[7] Vaithyanathan V, Chen L. Coarsening of ordered intermetallic precipitates with coherency stress. Acta Mater. 2002;50(16):4061–4073. doi:10.1016/S1359-6454(02)00204-5

[8] Zhang JX, Wang JC, Harada H, et al. The effect of lattice misfit on the dislocation motion in superalloys during high-temperature low-stress creep. Acta Mater. 2005;53(17):4623–4633. doi:10.1016/j.actamat.2005.06.013

[9] Link T, Epishin A, Fedelich B. Inhomogeneity of misfit stresses in nickel-base superalloys: effect on propagation of matrix dislocation loops. Philos Mag. 2009;89(13):1141–1159. doi:10.1080/14786430902877810

[10] Arora K, Kishida K, Tanaka K, et al. Effects of lattice misfit on plastic deformation behavior of single-crystalline micropillars of Ni-based superalloys. Acta Mater. 2017;138:119–130. doi:10.1016/j.actamat.2017.07.044

[11] Withers PJ, Bhadeshia H. Residual stress. Part 1–measurement techniques. Mater Sci Technol. 2001;17(4):355–365. doi:10.1179/026708301101509980

[12] Noyan IC, Cohen JB. Residual stress: measurement by diffraction and interpretation. New York (NY): Springer; 2013.

[13] Hemmersmeier U, Feller-Kniepmeier M. Element distribution in the macro-and microstructure of nickel base superalloy CMSX-4. Mater Sci Eng A. 1998;248(1-2):87–97. doi:10.1016/S0921-5093(98)00516-4

[14] Schulze C, Feller-Kniepmeier M. Transmisson electron microscopy of phase composition and lattice misfit in the Re-containing nickel-base superalloy CMSX-10. Mater Sci Eng A. 2000;281(1-2):204–212. doi:10.1016/S0921-5093(99)00713-3

[15] Kearsey R, Beddoes J, Jaansalu K, et al. The effects of Re, W and Ru on microsegregation behaviour in single crystal superalloy systems. Superalloys. 2004;2004:801–810. doi:10.7449/2004/Superalloys_2004_801_810.

[16] Dubiel B, Kalemba-Rec I, Kruk A, et al. Influence of high-temperature annealing on morphological and compositional changes of phases in Ni-base single crystal superalloy. Mater Charact. 2017;131:266–276. doi:10.1016/j.matchar.2017.07.021

[17] Fuchs G. Solution heat treatment response of a third generation single crystal Ni-base superalloy. Mater Sci Eng A. 2001;300(1-2):52–60. doi:10.1016/S0921-5093(00)01776-7

[18] Goerler J, Lopez-Galilea I, Roncery LM, et al. Topological phase inversion after long-term thermal exposure of nickel-base superalloys: experiment and phase-field

simulation. Acta Mater. 2017;124:151–158. doi:10.1016/j.actamat.2016.10.059
[19] Milhet X, Arnoux M, Cormier J, et al. On the influence of the dendritic structure on the creep behavior of a Re-containing superalloy at high temperature/low stress. Mater Sci Eng A. 2012;546:139–145. doi:10.1016/j.msea.2012.03.041
[20] Epishin A, Link T, Brückner U, et al. Effects of segregation in nickel-base superalloys: dendritic stresses. Superalloys. 2004;2004:537–543. doi:10.7449/2004/Superalloys_2004_537_543.
[21] Zhou Z, Li R, Wang Y, et al. Microscopic heterogeneity of low cyclic fatigue damage in Ni-based single crystal superalloy DD413. Mater Charact. 2024;207:113551. doi:10.1016/j.matchar.2023.113551
[22] Chen K, Huang R, Li Y, et al. Rafting-enabled recovery avoids recrystallization in 3D-printing-repaired single-crystal superalloys. Adv Mater. 2020;32(12):1907164. doi:10.1002/adma.201907164
[23] Lin S, Chen K, He W, et al. Custom-designed heat treatment simultaneously resolves multiple challenges facing 3D-printed single-crystal superalloys. Mater Design. 2022;222:111075. doi:10.1016/j.matdes.2022.111075
[24] Lin S, Chen K, Zeng Q, et al. A method for increasing the supersolvus critical strain for recrystallization in single-crystal superalloys. Mater Res Lett. 2023;11(10):856–862. doi:10.1080/21663831.2023.2253267
[25] Zhang H, Chen K, Lin S, et al. Recovery facilitated by interphase boundary motion circumvents recrystallization in superalloy single crystals. Mater Res Lett. 2024;12(3):180–189. doi:10.1080/21663831.2024.2312146
[26] Schmidt R, Feller-Kniepmeier M. Effect of heat treatments on phase chemistry of the nickel-base superalloy SRR 99. Metall Trans A. 1992;23(3):745–757. doi:10.1007/BF02675552
[27] Zhang M, Li L, Ding J, et al. Temperature-dependent micromechanical behavior of medium-Mn transformation-induced-plasticity steel studied by in situ synchrotron X-ray diffraction. Acta Mater. 2017;141:294–303. doi:10.1016/j.actamat.2017.09.030
[28] Li R, Xie Q, Wang Y-D, et al. Unraveling submicron-scale mechanical heterogeneity by three-dimensional X-ray microdiffraction. Proc Natl Acad Sci USA. 2018;115(3):483–488. doi:10.1073/pnas.1711994115
[29] Chen H, Wang Y-D, Nie Z, et al. Unprecedented non-hysteretic superelasticity of [001]-oriented NiCoFeGa single crystals. Nat Mater. 2020;19(7):712–718. doi:10.1038/s41563-020-0645-4
[30] Zhou G, Pantleon W, Xu R, et al. Quantification of local dislocation density using 3D synchrotron monochromatic X-ray microdiffraction. Mater Res Lett. 2021;9(4):182–188. doi:10.1080/21663831.2020.1862932
[31] Shen H, Chen K, Kou J, et al. Spatiotemporal mapping of microscopic strains and defects to reveal Li-dendrite-induced failure in all-solid-state batteries. Mater Today. 2022;57:180–191. doi:10.1016/j.mattod.2022.06.005
[32] Jia Z, Shen H, Kou J, et al. Solid electrolyte bimodal grain structures for improved cycling performance. Adv Mater. 2024: 2309019. doi:10.1002/adma.202309019
[33] Kou J, Chen K. PYXIS: an integrated software package for synchrotron micro/nano diffraction data analysis. J Appl Crystallogr. 2024;57:539-551. doi:10.1107/S1600576724000517
[34] Xuan G, Zhang W, Chai P, editors. EM algorithms of Gaussian mixture model and hidden Markov model. In: Dillene Mercer, editor. Proceedings 2001 International Conference on Image Processing (Cat. No. 01CH37205); 2001 Oct 7–10; Thessaloniki, Greece. Vol. I. New York (NY): IEEE Press; 2001. p. 145–148.
[35] Heckl A, Neumeier S, Göken M, et al. The effect of Re and Ru on γ/γ' microstructure, γ-solid solution strengthening and creep strength in nickel-base superalloys. Mater Sci Eng A. 2011;528(9):3435–3444. doi:10.1016/j.msea.2011.01.023
[36] Bruno G, Schumacher G, Pinto HC, et al. Measurement of the lattice misfit of the nickel-base superalloy SC16 by high-energy synchrotron radiation. Metall Trans A. 2003;34:193–197. doi:10.1007/s11661-003-0321-8
[37] Zenk CH, Povstugar I, Li R, et al. A novel type of Co–Ti–Cr-base γ/γ' superalloys with low mass density. Acta Mater. 2017;135:244–251. doi:10.1016/j.actamat.2017.06.024
[38] Neumeier S, Pyczak F, Göken M. The temperature dependent lattice misfit of rhenium and ruthenium containing nickel-base superalloys–experiment and modelling. Mater Design. 2021;198:109362. doi:10.1016/j.matdes.2020.109362
[39] Zenk C, Neumeier S, Stone H, et al. Mechanical properties and lattice misfit of γ/γ' strengthened Co-base superalloys in the Co–W–Al–Ti quaternary system. Intermetallics. 2014;55:28–39. doi:10.1016/j.intermet.2014.07.006
[40] Siebörger D, Knake H, Glatzel U. Temperature dependence of the elastic moduli of the nickel-base superalloy CMSX-4 and its isolated phases. Mater Sci Eng A. 2001;298(1-2):26–33. doi:10.1016/S0921-5093(00)01318-6